

# **Elastocaloric Response of Isotropic Liquid Crystalline Elastomers**

Jeremy A. Herman, Jonathan D. Hoang, and Timothy J. White\*

Liquid crystalline elastomers (LCEs) are soft materials that associate order and deformation. Upon deformation, mechanically induced changes order affect entropy and can produce a caloric output (elastocaloric). Elastocaloric effects in materials continue to be considered for functional use as solid state refrigerants. Prior elastocaloric investigations of LCEs and related materials have measured ≈2 °C temperature changes upon deformation (100% strain). Here, the elastocaloric response of LCEs is explored that are prepared with a subambient nematic to isotropic transition temperature. These materials are referred as "isotropic" liquid crystalline elastomers. The LCEs are prepared by a two-step thiol-Michael/thiol-ene reaction. This polymer network chemistry enhances elastic recovery and reduces hysteresis compared to acrylate-based chemistries. The LCEs exhibit appreciable elastocaloric temperature changes upon deformation and recovery (>  $\pm$  3 °C, total  $\Delta T$  of 6 °C) to deformation driven by minimal force (<< 1 MPa). Notably, the strong association of deformation and order and the resulting temperature change attained at low force achieves a responsivity of 14 °C MPa<sup>-1</sup> which is seven times greater than natural rubber.

## 1. Introduction

Liquid crystalline elastomers (LCEs) have been considered for functional use in energy,<sup>[1,2]</sup> optics,<sup>[3-5]</sup> soft robotics,<sup>[6,7]</sup> and impact-resistance<sup>[8-10]</sup> due to their unique assimilation of order and mechanical properties. LCEs are lightly to moderately crosslinked polymer networks that retain the liquid crystalline phase typically imparted from the monomeric starting materials.<sup>[11]</sup> LCEs undergo order–disorder transitions upon heating, which disrupts the ability of the mesogenic segments to align. Numerous prior reports, including some recent examinations, have detailed approaches to shifting the transition

J. A. Herman, T. J. White Department of Chemical and Biological Engineering University of Colorado

Jennie Smoly Caruthers Biotechnology Building, 3415 Colorado Ave, Boulder, CO 80303, USA

E-mail: tim.white@colorado.edu

J. D. Hoang, T. J. White

Materials Science and Engineering Program

University of Colorado

Jennie Smoly Caruthers Biotechnology Building, 3415 Colorado Ave, Boulder, CO 80303, USA



The ORCID identification number(s) for the author(s) of this article can be found under https://doi.org/10.1002/smll.202400786

DOI: 10.1002/smll.202400786

temperature of LCEs to lower temperatures. [12,13] Of relevance to this examination, are reports that detail the integration of 4-(6-acryloyloxy)hexyloxy)phenyl-4-(6-(acryloyloxy)hexyloxy)benzoate as mesogenic units in LCEs. [14-16] Compared to LCEs prepared with the canonical liquid crystalline monomer 1,4-Bis-[4-(6-acryloyloxyhexyloxy)benzoyloxy]—2-methylbenzene, these materials shift and sharpen the thermotropic transition.

This examination is generally concerned with exploring the elastocaloric response in LCEs. An elastocaloric material emits heat (e.g., a temperature increase) when subject to mechanical deformation. The thermodynamics of the process are well-established.<sup>[17–19]</sup> Although the caloric response of materials has been long studied (since Gough),<sup>[20]</sup> motivated by potential use in refrigeration the mechanical (elastocaloric),<sup>[21–26]</sup> electrical (electrocaloric),<sup>[27–31]</sup> and magnetic (magnetocaloric)<sup>[32–35]</sup> caloric effects have

been topics of considerable recent interest. Although Gough and early examinations focused on natural rubber, more recently, the elastocaloric effect has been extended to other materials, most notably shape memory alloys (SMAs). Like natural rubber, SMAs can undergo phase transformation accompanying deformation. The SMA nitinol has been extensively examined in these prior reports to exhibit a mechanically induced first-order austenite to martensite transition that can produce a temperature increase of 30 °C.[25,36,37] However, the mechanical properties of metals require large force inputs to achieve mechanical phase transition. Of soft materials, natural rubber (NR) remains an exemplar material and can achieve a moderate temperature increase (10 °C) with only several MPa of input stress. [24,38,39] The elastocaloric response of NR proceeds by strain-induced crystallization. The conversion from amorphous to semi-crystalline occurs at very large strains (> 500%). [40] The elastocaloric effect of NR is also temperature-dependent, achieving larger temperature changes at lower temperatures.[41]

Recent theoretical and experimental studies have considered LCEs as elastocaloric materials.  $^{[1,2,27,42]}$  Initial studies detail temperature changes of 1–2 °C at low-stress values (<< 1 MPa). Computation has suggested that LCEs can achieve even higher temperature changes (10 °C).  $^{[43]}$  We recently reported on a newly discovered phase transition in polymer networks containing appreciable liquid crystalline (LC) content.  $^{[44,45]}$  These materials do not

16136829, 2024, 32, Downloaded from https://onlinelibrary.wiley.com/doi/10.1002/smll.202400786 by Timothy White - University Of Colorado Boulder, Wiley Online Library on [14/10/2025]. See the Terms and Conditions

and-conditions) on Wiley Online Library for rules of use; OA articles are governed by the applicable Creative Commons

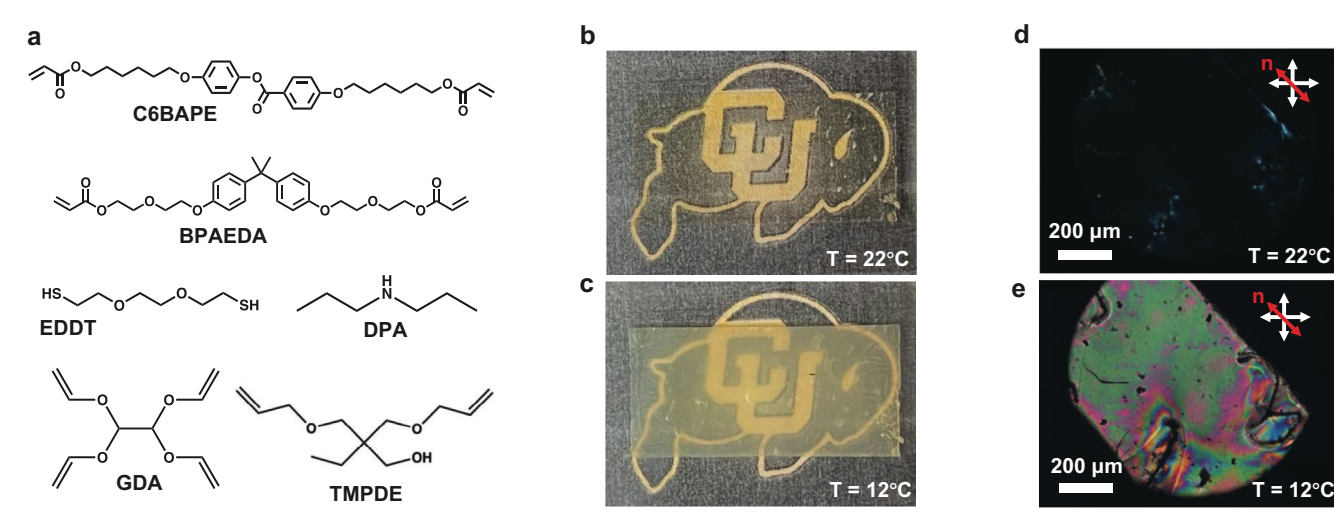


Figure 1. a) Chemical structures of diacrylate, thiol, vinyl, and amine monomers used in this report. b) Image taken above  $T_{\rm NI}$  at room temperature where the material appears optically transparent. c) Image taken below TNI where the material appears optically opaque as it becomes polydomain. d) Polarized optical micrographs showing no birefringence at room temperature above  $T_{NI}$ . e) Below the  $T_{NI}$  the material now displays birefringence in the polarized optical micrograph.

exhibit an LC phase upon preparation at any temperature and are not LCEs but amorphous polymers. Upon deformation, the embedded mesogens in these materials align to the direction of stretch and form an LC phase that we refer to as a mechanotropic phase transition. This phase transition was recently shown to also exhibit an elastocaloric.[1] To small strain (100%) and minimal stress (≈2 MPa), mechanotropic phase transitions in amorphous materials exhibited a small temperature change ( $\approx$ 2 °C).

The magnitude of the elastocaloric temperature change achievable in liquid crystalline systems is associated with the coupling of order and deformation. Extensive fundamental studies generally confirm that the magnitude of the orientation parameter for a given material system is maximized by the amount of liquid crystalline molecules in the composition. To achieve an amorphous state in our original studies, we copolymerized a moderate concentration of nonliquid crystalline monomer with liquid crystalline monomers.[1,44,45]

Here, we report on a new class of unaligned LCEs with nematic to isotropic transition temperatures ( $T_{\rm NI}$ 's) below room temperature that have near-maximal liquid crystalline content and excellent elastic recovery properties. These materials achieve larger and more efficient elastocaloric temperature changes compared to our prior examination of mechanotropic phase transitions in related materials. We utilize a two-step thiol-Michael/thiol-ene materials chemistry based on a two-phenyl ring liquid crystalline mesogen to create LCEs with  $T_{\rm NI}$ 's below room temperature. The polymer network is based on thiol-ene polymerization resulting in more homogenous distribution of crosslinking.[46-48] Since these particular materials exhibit an LC phase at subambient temperatures, we refer to these materials isotropic liquid crystalline elastomers (IsoLCEs). Notably, the IsoLCEs contain maximal LC content which is expected to enhance the coupling of deformation and order (entropy). The integration of thiol-ene polymerization as the basis for the network improves the elastic recovery of these materials which enhances the caloric performance. The elastocaloric response of the IsoLCEs is shown to exceed > 3 °C temperature changes at extremely small stress and strain values.

#### 2. Results and Discussion

The liquid crystalline (LC) materials examined here were prepared from compositions with a range of concentrations of liquid crystalline monomer (LCM). The isotropic liquid crystalline elastomers (IsoLCEs) were prepared by a two-step thiol-Michael/thiol-ene chemistry.[12,49] This examination utilizes the LCM C6BAPE (Figure 1a). [14-16] NMR spectra on this monomer is shown in Figure S1a (Supporting Information). When necessary, the LC content is diluted by incorporation of the monomer bisphenol A ethoxylate diacrylate (BPAEDA, Figure 1a). Thiol-Michael oligomerization of C6BAPE, BPAEDA, and the chain extending dithiol 2,2'-(Ethylenedioxy)diethanethiol (EDDT, Figure 1a) was catalyzed with dipropylamine (DPA, Figure 1a). By utilizing a molar excess of thiols, the thiol-Michael addition reaction produces thiol-terminated oligomers. Subsequently, the material system was subject to photoinitiated thiolene polymerization between the oligomeric dithiols and the vinyl crosslinker glyoxal bis(diallyl acetal) (GDA, Figure 1a). To elucidate the contribution of crosslink density, IsoLCE samples were prepared by introducing the divinyl molecule trimethylolpropane diallyl ether (TMPDE, Figure 1a) in place of GDA. The relative concentration of C6BAPE was varied by modifying the molar ratios of functional groups, the inclusion of BPAEDA, or replacing GDA content with TMPDE. The molar ratios of the compositions are specified in the Experimental Section. Samples will be referred to as  $IsoLCEXX_{\gamma\gamma}$  where XX is the mole fraction of LC content and YY is the mole fraction of GDA crosslinking content. The composition and material properties are summarized in Table 1.

Motivated by a recent report, these compositions exhibit nematic to isotropic transition temperatures ( $T_{NI}$ 's) below ambient temperature. Accordingly, the polymerization of these materials

16136829, 2024, 32, Downbaded from https://onlinelibrary.wiley.com/doi/10.1002/sml1.202400786 by Timothy White - University Of Colorado Boulder, Wiley Online Library on [14/10/2025]. See the Terms and Conditions (https://onlinelibrary.

and-conditions) on Wiley Online Library for rules of use; OA articles are governed by the applicable Creative Commons

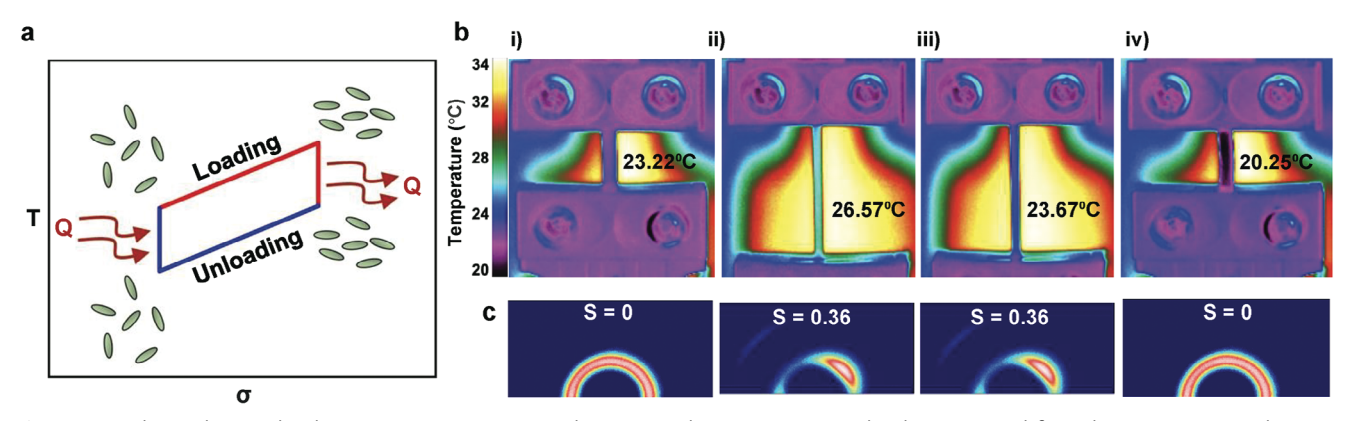


Figure 2. a) Elastocaloric cycle where temperature increases/decreases with stress. Heat is either lost or gained from the environment in between loading and unloading steps. Representation of LC network is inset for each cycle step. b) FLIR images taken during varying time points for IsoLCE44<sub>8.3</sub>. The sample's measured temperature is inset in each image. c) WAXS patterns taken during each elastocaloric step. Calculated Herman's orientation parameters are inset.

was done in the isotropic state and not subject to alignment. Prior examinations have prepared LCEs by polymerizing above the  $T_{\rm NI}$  of the mixture (by heating) to form so-called isotropic genesis polydomain LCE. Isotropic genesis polydomain LCEs are typically optical opaque at the macroscale but exhibit small microscale birefringent domains. The IsoLCE materials examined here were imaged and subject to polarized optical microscopy (Figure 1b,d). Notably, the IsoLCEs are optically clear and do not exhibit any domains even at high magnification. Upon cooling these materials, they become opaque (Figure 1c), and exhibit microscale birefringence (Figure 1e) associated with the polydomain state. The  $T_{NI}$  for the materials prepared here is reported in Table 1. Associated DSC thermograms are presented in the Supporting Information. Accordingly, these materials should be considered analogous to isotropic genesis polydomain LCE but in the ambient experiments, are in the "isotropic" state (hence the phrasing, isotropic LCE).

Informed by our previous study of mechanotropic phase transitions in related materials capable of mechanically induced isotropic to liquid crystalline phase transitions, we hypothesized

**Table 1.** Material properties of all networks with varying LC and crosslinking content. Iso represents the isotropic state these materials are in upon preparation since at room temperature every network is above its  $T_{\rm NI}$ .

Sample Name	LC Content [mol%]	GDA Content [mol%]	T <sub>g</sub> [°C]	T <sub>NI</sub> [°C]	Modulus [MPa]
IsoLCE37 <sub>16.7</sub>	37	16.7	-39	3	1.3
IsoLCE37 <sub>11.6</sub>	37	11.6	-39	0.5	1.3
IsoLCE37 <sub>6.5</sub>	37	6.5	-41	-0.3	0.8
IsoLCE42 <sub>11.5</sub>	42	11.5	-38	8	0.93
IsoLCE42 <sub>9</sub>	42	9	-38	8	1
IsoLCE42 <sub>6.5</sub>	42	6.5	-35	6	0.9
IsoLCE44 <sub>8.3</sub>	44	8.3	-37	15	0.64
IsoLCE44 <sub>7.4</sub>	44	7.4	-37	14	0.6
IsoLCE44 <sub>6.5</sub>	44	6.5	-35	14	0.6
IsoLCE46 <sub>6.5</sub>	46	6.5	-35	18	0.59

that IsoLCEs may also be compelling elastocaloric materials. The proposed elastocaloric cycle and the associated LC network orientation are illustrated in Figure 2a. Applied stress is expected to align the materials and realize an initial increase in temperature. As the network is aligned, heat (Q) is lost to the environment and the sample returns to ambient temperature. Releasing the deformation allows the material to recover the disordered state, accompanied by a decrease in temperature. Again, elastocaloric heating and cooling are adiabatic processes (e.g., the total entropy of the system is zero). Upon deformation, the IsoLCE materials undergo a disorder-to-order transition (decrease in configurational entropy). The ordered state is associated with the preferential orientation of the liquid crystalline segments in the material to align. This change in entropy is offset by a temperature increase (e.g., thermal entropy). When the IsoLCE is unloaded, the material recovers the disordered state (increase in configurational entropy) that is accompanied by a temperature decrease.

The proposed elastocaloric response of IsoLCE was confirmed by FLIR imaging presented in Figure 2b for IsoLCE4483. Here, the material was subject to rapid deformation to 150% strain. Upon deformation, the material exhibits a 3.35 °C increase in temperature. To sustain deformation, the material recovers to room temperature. Upon releasing the deformation, the material exhibits a −3.42 °C decrease in temperature before recovering to ambient temperature. To confirm the association of deformation and order (entropy), we utilized wide-angle X-ray scattering (WAXS) to monitor orientational order parameter changes during deformation (Figure 2c). As expected, upon deformation, IsoLCE4483 orients when deformed (to an orientation parameter of 0.36) and recovers the disordered state upon release. As an adiabatic elastocaloric process, the total entropy change in the network is zero. Accordingly, the decrease in configurational entropy (e.g., the mechanically induced orientation) must be accompanied by an increase in the thermal entropy of the system.<sup>[19]</sup> Similarly, when the material recovers to the isotropic state, the increase in configurational entropy is offset by the decrease in thermal entropy of the system.

The elastocaloric temperature profile for  $IsoLCE44_{8.3}$  when instantaneously stretched to 150% strain and subsequently released is shown in **Figure 3a**. This temperature profile is taken

16136829, 2024, 32, Downloaded from https://onlinelibrary.wiley.com/doi/10.1002/sml1.202400786 by Timothy White - University Of Colorado Boulder, Wiley Online Library on [14/10/2025]. See the Terms and Conditions (https://onlinelibrary.wiley.com/

nd-conditions) on Wiley Online Library for rules of use; OA articles are governed by the applicable Creative Commons

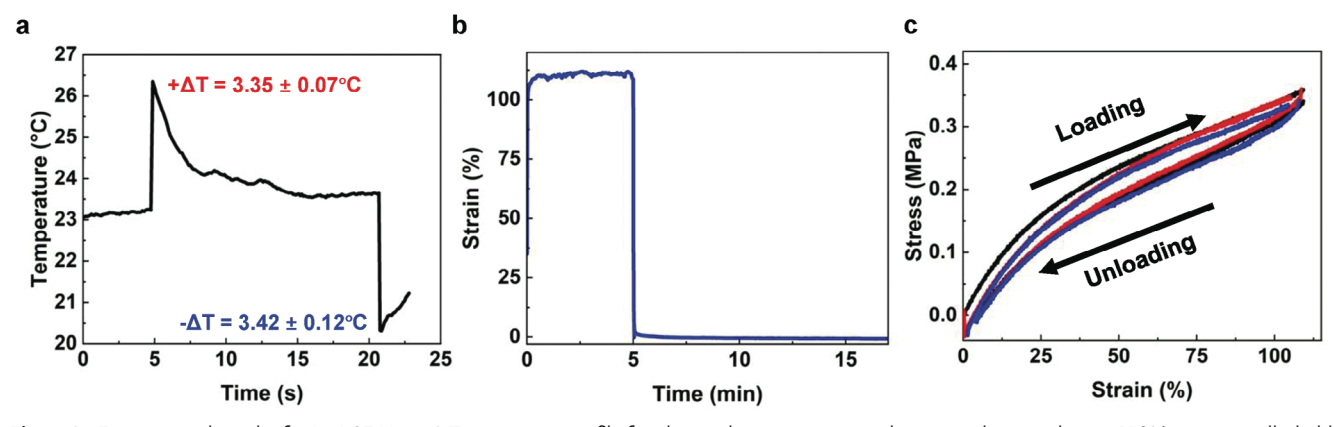


**Figure 3.** Experimental results for IsoLCE44<sub>8,3</sub>. a) Temperature profile for elastocaloric experiment where sample was taken to 150% strain rapidly, held for 15 s, and then rapidly taken to 0% strain. Calculated increasing and decreasing temperatures are inset. b) Creep-recovery experiment where the sample was rapidly loaded, held for 5 min, and then allowed to recovery for an extended period of time. c) Tensile loading and unloading cycles to show mechanical hysteresis.

from the thermal imaging (Video S1, Supporting Information). The temporal response of the temperature change seems to mirror the deformation, with a near-instantaneous temperature rise.

Compared to our recent examination of mechanotropic phase transitions, the IsoLCE material exhibits a larger temperature change. Further, unlike the previous acrylate-based material, this composition has near-identical temperature increase and decrease. To better understand the mechanical deformation of this material and associated mechanical response, we subjected the material to creep recovery and hysteresis measurements. As presented in Figure 3b, the material was held in tension at a constant stress, the stress is then removed, and the material was allowed to recover. The amount of stress imparted on the network is derived from its room temperature tensile test (Figure S4b, Supporting Information). The material has a near-instantaneous recovery time, considerably improved from the prior report. Further, IsoLCE4483 was subjected to repeated deformation cycles to 100% strain and back (Figure 3c). As in typical material loading and unloading cycles, this network has a softer response upon unloading. However, the loading and unloading curves are nearly identical and the differences only add up to 10% hysteresis. The low mechanical hysteresis of these materials results in minimal variability in the elastocaloric response. Accordingly, the elastocaloric values reported are averages of at least five experiments. For example, the elastocaloric response of IsoLCE4483 is  $3.35 \pm 0.07$  °C (Figure 3a).

We now consider the impact of compositional factors such as crosslinking and LC content on elastocaloric output. Nine IsoLCE samples were prepared with either equivalent LC content and varied crosslinking or equivalent crosslinking and varied LC content. The primary crosslinking molecule in this study is the tetrafunctional vinyl crosslinker glyoxal bis(diallyl acetal) (GDA).

IsoLCE samples were formulated in stoichiometric ratios in which GDA was replaced with the difunctional vinyl monomer trimethylolpropane diallyl ether (TMPDE). As TMPDE concentration increases (and GDA decreases) in the mixtures, the crosslinker molar concentration decreases, but the overall liquid crystalline content remained constant. IsoLCEs could be prepared with as low as 6.5 mol% GDA. To isolate the contribution of LC content, the molar concentration of the crosslinker GDA

was held constant, and BPAEDA was substituted for C6BAPE. Figure 4 summarizes the characterization and response of the nine IsoLCE materials, presented in groupings defined by liquid crystalline concentrations: 37 mol% (Figure 4a-c), 42 mol% (Figure 4d-f), and 44 mol% (Figure 4g-i). Each set of materials was subject to creep recovery experiments. In all cases, increasing crosslinking (e.g., GDA concentration) reduces the amount of creep (Figure 4a,d,g). Short timescale recovery is evident in the insets in Figure 4a,d,g. In each sample series (e.g., 37, 42, and 44 mol% LC), the IsoLCEs with the highest crosslinker concentration have the fastest recovery rate. Hysteresis values were calculated from cyclic stress-strain deformations reported in Figures S2-S4 (Supporting Information). However, the highest hysteresis for the nine materials is 14.5%. A rubber band, for example, can exhibit 15% hysteresis when subjected to the same loading and unloading conditions (Figure \$7, Supporting Information). The elastocaloric response of these materials is summarized in Figure 4c,f,i (raw data found in Figures S2–S4, Supporting Information). All samples were rapidly strained to 100%, held for 15 s, and then released. Unlike our previous examination, all samples exhibit commensurate magnitude  $+\Delta T$  and  $-\Delta T$  upon deformation and recovery. Two conclusions can be drawn from these data: i) increasing crosslinking in these materials increases the magnitude of the achievable temperature change and ii) increasing the liquid crystalline concentration maximizes the amount of achievable temperature change. To isolate and emphasize the contribution of liquid crystalline content to the elastocaloric response, the data in Figure 4 is presented as a function of LC content at the maximum crosslinker concentration achievable in each formulation in Figure 5. A fourth sample is added to further extend the comparison, containing 46 mol% C6BAPE. As evident in Figure 4 and Figures S2–S6 (Supporting Information), all four samples exhibit limited creep and rapid recovery.

Figure 5a compares the elastocaloric temperature change of the four IsoLCE materials. This comparison indicates that increasing liquid crystalline content increases the magnitude of  $+\Delta T$  and  $-\Delta T$ . Notably, IsoLCE46<sub>6.5</sub> displays the largest temperature change almost reaching 3 °C when strained to 100%. This makes sense, as IsoLCE46<sub>6.5</sub>, comprised of the highest amount of LC content, can achieve the largest change in order which

16136829, 2024, 32, Downloa

nelibrary.wiley.com/doi/10.1002/sml1.202400786 by Timothy White - University Of Colorado Boulder

, Wiley Online Library on [14/10/2025]. See the Terms

on Wiley Online Library for rules of use; OA articles are governed by the applicable Creative Commons

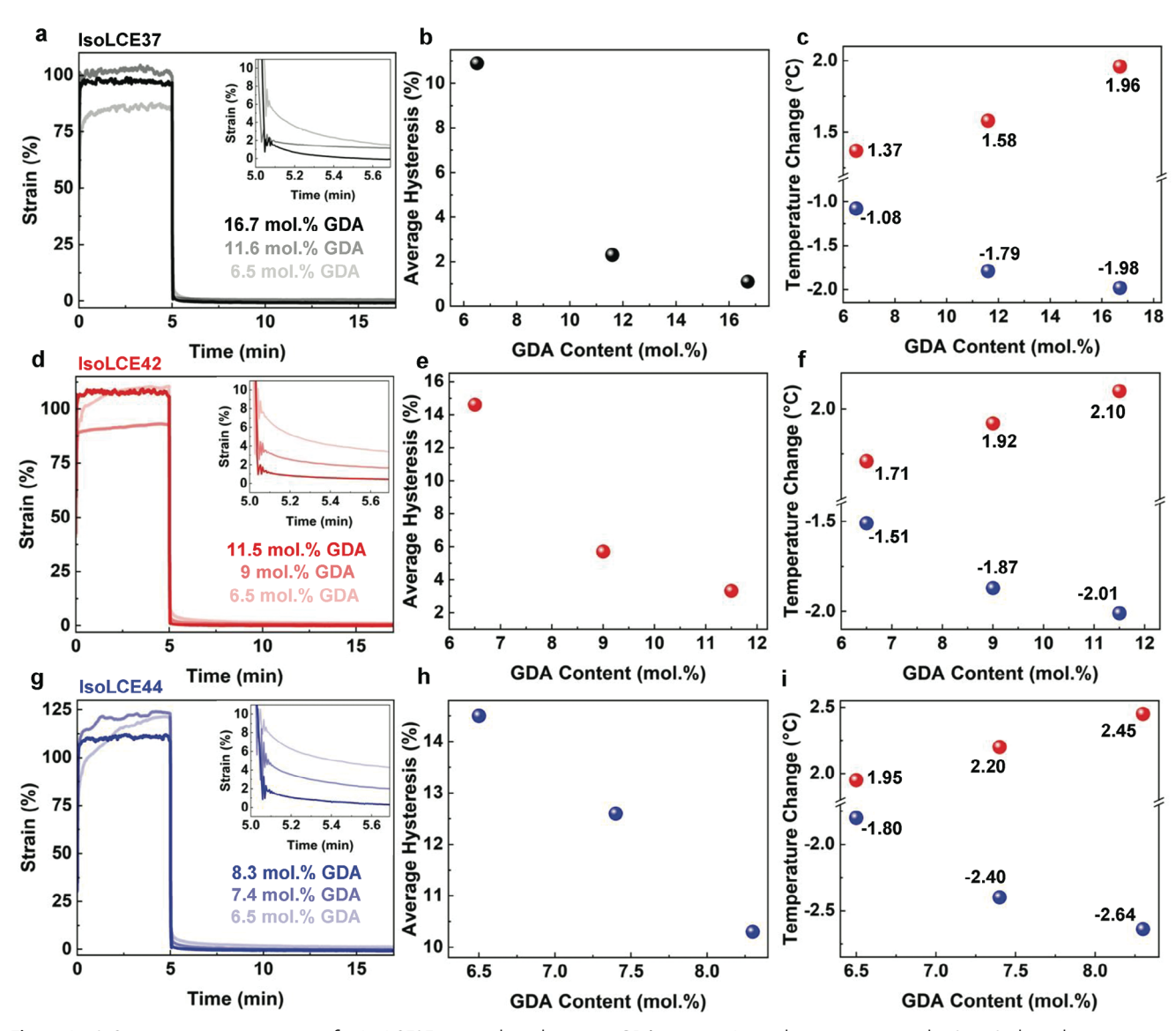


Figure 4. a) Creep-recovery experiments for IsoLCE37 materials with varying GDA content. Immediate recovery results (inset) show that recovery is dependent on crosslinking content. b) Average percent hysteresis for IsoLCE37 materials with varying GDA content showing how hysteresis decreases as crosslinking increases. c) Increasing and decreasing temperature changes for IsoLCE37 materials with varying GDA content. d) Creep-recovery experiments for IsoLCE42 materials with varying GDA content. e) Average percent hysteresis for IsoLCE42 materials. f) Increasing and decreasing temperature changes for IsoLCE44 materials. g) Creep-recovery experiments for IsoLCE44 materials with varying GDA content. h) Average percent hysteresis for IsoLCE44 materials. i) Increasing and decreasing temperature changes for IsoLCE44 materials. For further clarity, a–c) represent data for material IsoLCE37, d–f) represent data for material IsoLCE42, and g–i) represent data for material IsoLCE44.

corresponds to the largest temperature change upon deformation. However, the cooling temperature for IsoLCE46<sub>6.5</sub> is lower than expected. As summarized in Figure 5b, this sample has a significant increase in hysteresis which we suggest is at the root of the comparatively reduced  $-\Delta T$ . If the network cannot fully recover the disordered state (or does not rapidly recover full disordered state), the magnitude of the entropy change will be less and so will the corresponding  $-\Delta T$ . Generally, increasing LC content does increase the average hysteresis value (Figure 5b). This makes sense, as the deformation and recovery of materials with more LC units have a greater number of intermolecular forces to balance. With lower observed values, it does not seem that the

hysteresis affects the magnitude of the  $+\Delta T$  and  $-\Delta T$  in any of the materials but IsoLCE46<sub>6.5</sub>.

Comparatively, the magnitude of the temperature changes observed in the IsoLCEs fall short of the magnitude achieved in shape memory alloys (SMAs) like nitinol ( $\approx 30$  °C) or soft materials, like natural rubber (NR) ( $\approx 10$  °C). However, the elastocaloric response in these materials is distinctive, in that the temperature change is induced nearly instantaneously upon deformation to small force inputs. Comparatively, elastocaloric effects in SMAs can require upwards of 1 GPa of stress. Further, the deformation of NR often requires a minimum of 500% strain to initiate crystallization and an appreciable temperature change. The

16136829, 2024, 32, Downloaded from https://onlinelibrary.wiley.com/doi/10.1002/sml1.202400786 by Timothy White - University Of Colorado Boulder

, Wiley Online Library on [14/10/2025]. See the Terms and Condit

on Wiley Online Library for rules of use; OA articles are governed by the applicable Creative Commons

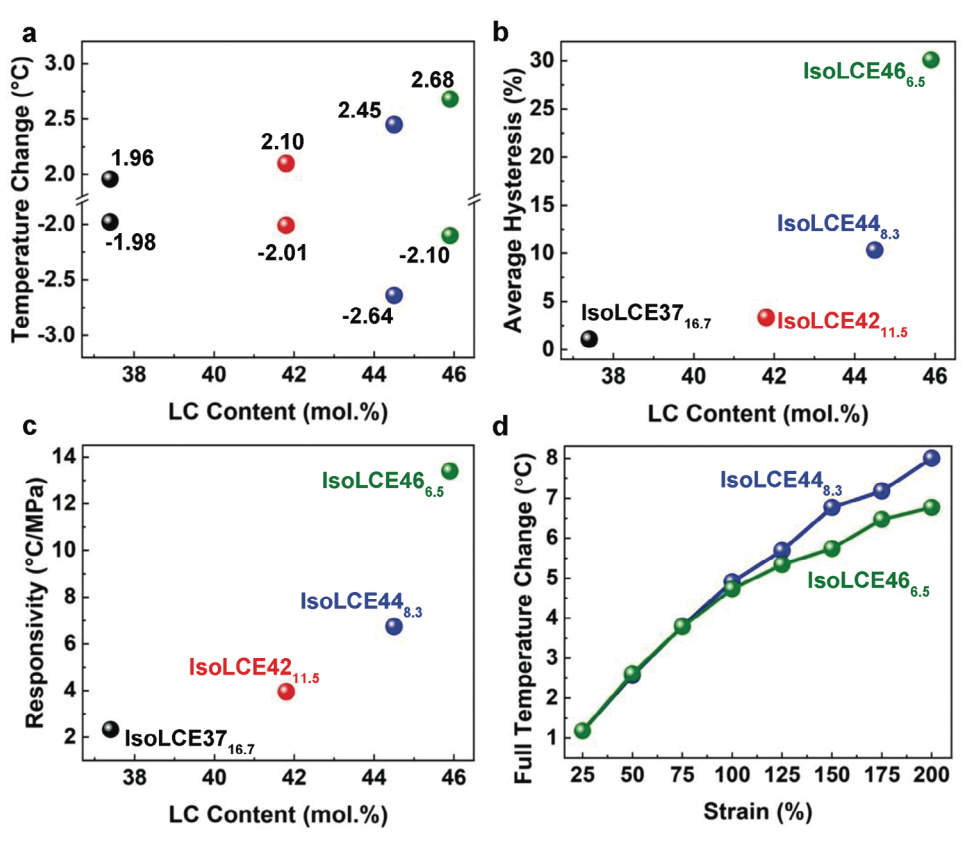


Figure 5. a) Increasing and decreasing temperature changes as a function of LC content and crosslinking for 100% strain experiments. Top data points correspond to increasing temperature upon loading while bottom data points correspond to decreasing temperature upon unloading. b) Average percent hysteresis for each network when loaded to 100% strain and back three times. c) Elastocaloric responsivity metric as a function of LC content for 100% strain experiments. d) Full temperature changes (increasing and decreasing together) for Iso-44<sub>8,3</sub> and Iso-46<sub>6,5</sub> for multiple strain values.

coupling of temperature change and force input is commonly ascribed as responsivity in elastocaloric materials. For reference, SMAs have responsivity around 0.05 °C MPa<sup>-1</sup> while NR has responsivity values ≈2 °C MPa<sup>-1</sup>. The calculated responsivities for the IsoLCE to 100% strain are shown in Figure 5c. All four samples shown here have responsivity values that exceed 2 °C MPa<sup>-1</sup>, with IsoLCE46<sub>65</sub> achieving nearly 14 °C MPa<sup>-1</sup>. The magnitude of the elastocaloric temperature change is also affected by the extent of the deformation. Figure 5d plots the full temperature change (e.g.,  $+\Delta T \pm \Delta T$ ) for IsoLCE44<sub>8,3</sub> and IsoLCE46<sub>6,5</sub> as a function of strain. The materials have effectively identical temperature changes at strains of 25%, 50%, and 75%. However, at 100% strain and above, the full temperature change associated with the deformation of IsoLCE46<sub>6.5</sub> is less than IsoLCE44<sub>8.3</sub>. Again, this is attributable to the reduction in  $-\Delta T$  due to hysteresis and recovery.

In Figure 6, the full temperature change (Figure 6a), responsivity (Figure 6b), and average hysteresis (Figure 6c) are plotted against LC content. LC content has a direct impact on each result as the materials with the highest LC content display the highest temperature changes, the highest responsivities, and the highest hysteresis. As discussed previously, a baseline crosslinking of 6.5 mol% GDA content was used for each set of materials since this was found to be the lowest GDA content that makes a cohesive film. These lowest crosslinked materials are plotted in purple

separately from the rest of the data to highlight their differences where the materials with the lowest crosslinking display the lowest temperature changes, the lowest responsivities, and the highest hysteresis. Finally, we plot the full temperature change, responsivity, and hysteresis against GDA content in Figure 6d,e,f, respectively. GDA content has a clear and significant effect on the full temperature change and average hysteresis as materials with higher crosslinking have higher temperature changes and lower hysteresis as discussed previously. The GDA content does not seem to have as significant of an effect on the responsivity as these values remain constant. These IsoLCEs demonstrate unique behavior among elastomers and their properties can easily be tailored to achieve a range of properties.

#### 3. Conclusion

This examination explores elastocaloric responses in LCEs prepared and tested in the isotropic state. Because of the low nematic to isotropic transition temperature of the formulations, these materials are isotropic at room temperature. The polymer network topology is analogous to isotropic genesis polydomain LCE, however, enabled by the low  $T_{\rm NI}$  of the LCE prepared here, caloric experiments are undertaken in the isotropic state. A systematic evaluation of LC content and network crosslinking illustrate the association of deformation, recovery, and caloric output.

16136829, 2024, 32, Downloaded from https

//onlinelibrary.wiley.com/doi/10.1002/sml1.202400786 by Timothy White - University Of Colorado Boulder , Wiley Online Library on [14/10/2025]. See the Terms and Conditions of Colorado Boulder , Wiley Online Library on [14/10/2025].

nd-conditions) on Wiley Online Library for rules of use; OA articles are governed by the applicable Creative Commons

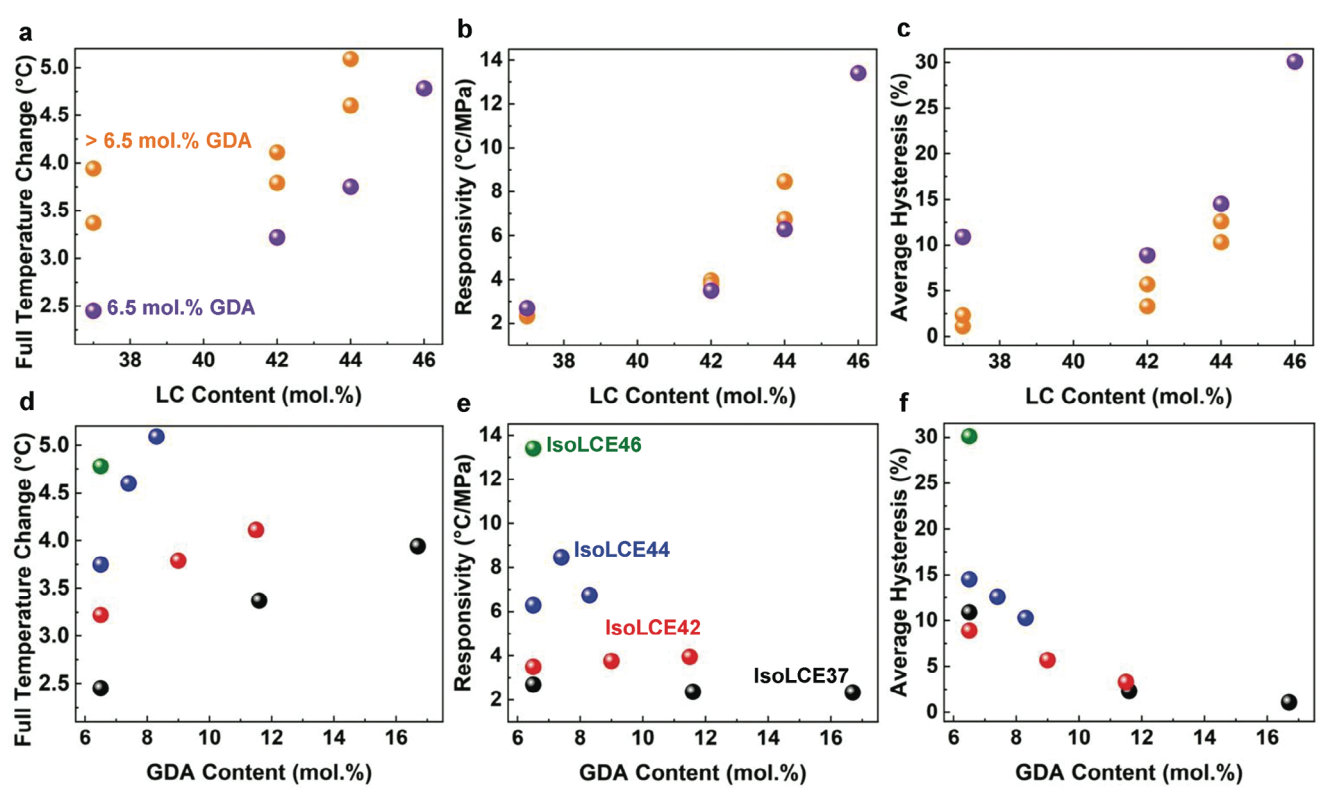


Figure 6. a) Summary of full temperature change measurements across all samples as a function of LC content. The samples with the lowest GDA crosslinking content (6.5 mol%) are plotted in purple while the rest that have more than 6.5 mol% GDA are plotted in orange. b) Calculated responsivity metric across all samples as a function of LC content. c) Average percent hysteresis for all samples as a function of LC content. The data is plotted this way to highlight the significance of LC content to elastocaloric results but also to show the coupling of crosslinking with LC content. d) Full temperature change measurements across all samples as a function of GDA crosslinking content. e) Calculated responsivity metric for all samples as a function of GDA crosslinking content. f) Average percent hysteresis for all samples as a function of GDA crosslinking content.

At minimal stress (<< 1 MPa) and strain (< 200%) imparted on these networks, they show an appreciable elastocaloric temperature change (> 3 °C) that is fully reversible across several cycles. A responsivity of as much as 14 °C MPa<sup>-1</sup> is observed. By examining the composition-structure relationships with correlation to the caloric output, this work establishes a foundational understanding for future research and advances the functional performance of these materials in applications such as solid state refrigeration.

## 4. Experimental Section

Materials: Compositions were based on the diacrylate liquid crystal monomer 4-(6-acryloyloxy) hexyloxy) phenyl-4-(6-(acryloyloxy)hexyloxy) benzoate (C6BAPE, Synthon). This monomer was oligomerized by thiol-Michael addition with the dithiol 2,2'-(ethylenedioxy) diethanethiol (EDDT, Aldrich). The thiol-Michael reaction is catalyzed by 1 wt% of the base catalyst dipropylamine (DPA, Aldrich). Photoinitiated crosslinking was facilitated by the inclusion of the tetrafunctional vinyl crosslinker glyoxal bis(diallyl acetal) (GDA, Aldrich). Photopolymerization was initiated by the inclusion of 2 wt% of 2-benzyl-2-dimethylamino-1-(4morpholinophenyl)-butanone-1 (Irgacure 369, IGM Resins). Finally, the radical inhibitor 4-methoxyphenol (MEHQ, Aldrich) was included at 1 wt% to suppress polymerization before light exposure. In samples where crosslinking was held constant but liquid crystalline content was changed, the nonliquid crystalline diacrylate monomer bisphenol A ethoxylate diacrylate (BPAEDA, Aldrich) was added. When crosslinking was changed by liquid crystalline content was held constant, the difunctional vinyl molecule trimethylolpropane diallyl ether (TMPDE, Aldrich)

Sample Preparation: All solid components (C6BAPE, BPAEDA, Irgacure 369, MEHQ) were melted and mixed in a glass vial. Liquid components (EDDT, GDA, TMPDE, DPA) were then added. The mole ratios of functional groups were adjusted to yield materials of varying LC content and crosslinking. After vortex mixing, each mixture is transferred onto a glass slide and sandwiched with another glass slide with 100 µm spacers in between to control sample thickness. The formulations were held at 100 °C for 3 h to facilitate the thiol-Michael reaction. After 3 h, the formulations were polymerized at 100  $^{\circ}$ C using a 365 nm light at 50 mW cm<sup>-2</sup> for 10 min. After polymerization, each formulation was cooled overnight before harvesting.

Characterization: Differential scanning calorimetry (DSC 2500-TA Instruments) was performed on each material formulation to assess any thermal transitions. A heat-cool-heat cycle was conducted with the heating rates set at 10 °C min<sup>-1</sup> and the cooling rate at 5 °C min<sup>-1</sup>. The second heating cycle is reported for each material. The glass transition temperature  $(T_{\sigma})$  is reported from the midpoint of the second-order endothermic transition while the nematic to isotropic transition temperatures  $(T_{NI})$  are reported from the location of the endothermic peak. Dynamic mechanical analysis (DMA 850-TA Instruments) was used for tensile, creep-recovery, hysteresis tests. Each sample was strained at 10% min<sup>-1</sup> for the initial tensile tests until material failure. Reported modulus values were calculated from the slope of the initial linear region in each tensile test. For creeprecovery studies, each material was held at a constant stress for 5 min. The stress values were chosen so that each material was pulled to  $\approx 100\%$ strain. The stress was removed after 5 min and the material was allowed

NANO · MICRO SMO

16136829, 2024, 32, Downloaded from https://onlinelibrary.wiley.com/doi/10.1002/smll.202400786 by Timothy White - University Of Colorado Boulder, Wiley Online Library on [14/10/2025]. See the Terms and Conditions

nd-conditions) on Wiley Online Library for rules of use; OA articles are governed by the applicable Creative Commons

to recover for 10 min. Hysteresis studies were conducted as three consecutive loading and unloading cycles at rates of 1000% min<sup>-1</sup>. The average hysteresis percentage was calculated using Equation 1.

Average Hysteresis (%) = 
$$\frac{\text{Area}_{\text{Loading}} - \text{Area}_{\text{Unloading}}}{\text{Area}_{\text{Loading}}} \times 100\%$$
 (1)

Polarized optical microscopy (POM) was used to visualize birefringence as a function of temperature while the temperature was controlled with an Instec cooling stage.

Elastocaloric Experiments: Strain was controlled using dynamic mechanical analysis (DMA 850–TA Instruments). Temperature changes were monitored and calculated using an infrared thermal imaging camera (FLIR). Samples were equilibrated at room temperature before being rapidly deformed to a set strain value. Samples were held under constant strain for 15 s where the strain was then rapidly released. All steps were monitored using the FLIR camera and temperature changes were calculated from the FLIR temperature gradients. The stress from each experiment was monitored using DMA 850 and was used to calculate each material's responsivity metric.

Wide Angle X-Ray Scattering (WAXS): X-ray diffraction patterns were taken on beamline 5-ID-D at the Advanced Photon Source (APS) at Argonne National Laboratory. Each scan consisted of a 1-s X-ray exposure with an energy of 17 keV. The strain was controlled using an Instron servohydraulic tensile stage. The experiments done here mimic elastocaloric experiments where the sample is rapidly deformed to a set strain, held in tension for 15 s, and then strain is rapidly released. X-ray scans are taken before straining, immediately upon application of strain, throughout the isostrain experiment, and then immediately upon removal of strain.

## **Supporting Information**

Supporting Information is available from the Wiley Online Library or from the author.

## Acknowledgements

This work was supported in part by the Petroleum Research Fund of the American Chemical Society. J.A.H. acknowledges support from the National Science Foundation via a Graduate Research Fellowship. The authors acknowledge beamline 5-ID-D at Argonne National Lab for their help in collecting WAXS patterns and for the use of their facilities. The authors acknowledge David Kennedy for helping in gathering the NMR spectra.

#### **Conflict of Interest**

The authors declare no conflict of interest.

### **Data Availability Statement**

The data that support the findings of this study are available from the corresponding author upon reasonable request.

# Keywords

elastocaloric, liquid crystalline elastomers, materials chemistry

Received: February 2, 2024 Revised: February 28, 2024 Published online: March 20, 2024

- J. A. Koch, J. A. Herman, T. J. White, Phys. Rev. Mater. 2021, 5, 62401.
- [2] M. Lavrič, N. Derets, D. Črešnar, V. Cresta, V. Domenici, A. Rešetič, G. Skačej, M. Sluban, P. Umek, B. Zalar, Z. Kutnjak, B. Rožič, *Liq. Cryst.* 2020. 43. 405.
- [3] M. T. Brannum, A. M. Steele, M. C. Venetos, L. S. T. J. Korley, G. E. Wnek, T. J. White, Adv. Opt. Mater. 2019, 7, 1801683.
- [4] K. R. Schlafmann, T. J. White, Nat. Commun. 2021, 12, 4916.
- [5] A. T. Phillips, K. R. Schlafmann, H. E. Fowler, T. J. White, Adv. Opt. Mater. 2022, 10, 2201457.
- [6] Y.-C. Wang, Y.-Z. Wang, J.-C. Shu, W.-Q. Cao, C.-S. Li, M.-S. Cao, Adv. Funct. Mater. 2023, 33, 2303560.
- [7] Y. Shang, J. Wang, T. Ikeda, L. Jiang, J. Mater. Chem. C. 2019, 7, 3413.
- [8] M. O. Saed, W. Elmadih, A. Terentjev, D. Chronopoulos, D. Williamson, E. M. Terentjev, Nat. Commun. 2021, 12, 6676.
- [9] N. A. Traugutt, D. Mistry, C. Luo, K. Yu, Q. Ge, C. M. Yakacki, Adv. Mater. 2020, 32, 2000797.
- [10] C. Luo, C. Chung, N. A. Traugutt, C. M. Yakacki, K. N. Long, K. Yu, ACS Appl. Mater. Interfaces 2021, 13, 12698.
- [11] T. J. White, D. J. Broer, Nature Mater 2015, 14, 1087.
- [12] M. O. Saed, C. P. Ambulo, H. Kim, R. De, V. Raval, K. Searles, D. A. Siddiqui, J. M. O. Cue, M. C. Stefan, M. R. Shankar, T. H. Ware, Adv. Funct. Mater. 2019, 29, 1806412.
- [13] R. K. Shaha, A. H. Torbati, C. P. Frick, J. Appl. Polym. Sci. 2021, 138, 50135.
- [14] J. M. McCracken, B. R. Donovan, K. M. Lynch, T. J. White, J. M. McCracken, B. R. Donovan, K. M. Lynch, T. J. White, Adv. Funct. Mater. 2021, 31, 2100564.
- [15] T. S. Hebner, C. N. Bowman, T. J. White, Polym. Chem. 2021, 12, 1581.
- [16] G. E. Bauman, J. M. McCracken, T. J. White, Angew. Chem., Int. Ed. 2022, 61, 202202577.
- [17] J. Tušek, K. Engelbrecht, R. Millán-Solsona, L. Mañosa, E. Vives, L. P. Mikkelsen, N. J. Pryds Tušek, K. Engelbrecht, N. Pryds, R. Millán-Solsona, L. Mañosa, E. Vives, L. P. Mikkelsen, Adv. Energy Mater. 2015, 5, 1500361.
- [18] X. Moya, N. D. Mathur, Science 2020, 370, 797.
- [19] S. Qian, Y. Geng, Y. Wang, J. Ling, Y. Hwang, R. Radermacher, I. Takeuchi, J. Cui, Int. J. Refrigerat. 2016, 64, 1.
- [20] V. I. I. Holme, Philos. Mag. 1806, 24, 39.
- [21] G. Coativy, H. Haissoune, L. Seveyrat, G. Sebald, L. Chazeau, J. M. Chenal, L. Lebrun, Appl. Phys. Lett. 2020, 117, 193903.
- [22] J. Tušek, K. Engelbrecht, D. Eriksen, S. Dall'Olio, J. Tušek, N. Pryds, Nat. Energy 2016, 1, 16134.
- [23] Y. Yoshida, K. Yuse, D. Guyomar, J. F. Capsal, G. Sebald, Appl. Phys. Lett. 2016, 108, 242904.
- [24] N. Candau, E. Vives, A. I. Fernández, M. L. Maspoch, *Polymer* 2021, 236, 124309.
- [25] D. Cong, W. Xiong, A. Planes, Y. Ren, L. Mañosa, P. Cao, Z. Nie, X. Sun, Z. Yang, X. Hong, Y. Wang, Phys. Rev. Lett. 2019, 122, 255703.
- [26] F. Greibich, R. Schwödiauer, G. Mao, D. Wirthl, M. Drack, R. Baumgartner, A. Kogler, J. Stadlbauer, S. Bauer, N. Arnold, M. Kaltenbrunner, Nat. Energy 2021, 6, 260.
- [27] M. Trček, M. Lavrič, G. Cordoyiannis, B. Zalar, B. Rožič, S. Kralj, V. Tzitzios, G. Nounesis, Z. Kutnjak, *Philos. Trans. R. Soc., A* 2016, 374, 20150301.
- [28] E. Defay, R. Faye, G. Despesse, H. Strozyk, D. Sette, S. Crossley, X. Moya, N. D. Mathur, *Nature Commun* 2018, 9, 1827.
- [29] Y. Wang, Z. Zhang, T. Usui, M. Benedict, S. Hirose, J. Lee, J. Kalb, D. Schwartz, Science 2020, 370, 129.
- [30] X. Qian, D. Han, L. Zheng, J. Chen, M. Tyagi, Q. Li, F. Du, S. Zheng, X. Huang, S. Zhang, J. Shi, H. Huang, X. Shi, J. Chen, H. Qin, J. Bernholc, X. Chen, L.-Q. Chen, L. Hong, Q. M. Zhang, *Nature* 2021, 600, 664.
- [31] B. Lu, X. Chen, T. Zhang, S. G. Lu, Q. M. Zhang, Appl. Phys. Lett. 2018, 113, 153903.

www.advancedsciencenews.com

www.small-journal.com

16136829, 2024, 32, Downloaded from https://onlinelibrary.wiley.com/doi/10.1002/sml1.202400786 by Timothy White - University Of Colorado Boulder

, Wiley Online Library on [14/10/2025]. See the Terms

are governed by the applicable Creative Commons

- [32] C. L. Zhang, H. F. Shi, E. J. Ye, Y. G. Nie, Z. D. Han, B. Qian, D. H. Wang, Appl. Phys. Lett. 2015, 107, 212403.
- [33] O. Gutfleisch, T. Gottschall, M. Fries, D. Benke, I. Radulov, K. P. Skokov, H. Wende, M. Gruner, M. Acet, P. Entel, M. Farle, Philos. Trans. R. Soc., A 2016, 374, 20150308.
- [34] J. Liu, T. Gottschall, K. P. Skokov, J. D. Moore, O. Gutfleisch, Nat. Mater. 2012, 11, 620.
- [35] Y. Zhang, L. Hou, Z. Ren, X. Li, G. Wilde, J. Alloys Compd. 2015, 656,
- [36] E. Bonnot, R. Romero, L. Mañosa, E. Vives, A. Planes, Phys. Rev. Lett. 2007, 100, 125901.
- [37] G. J. Pataky, E. Ertekin, H. Sehitoglu, Acta. Mater. 2015, 96, 420.
- [38] Z. Xie, G. Sebald, D. Guyomar, Appl. Phys. Lett. 2016, 108, 041901.
- [39] D. Guyomar, Y. Li, G. Sebald, P. J. Cottinet, B. Ducharne, J. F. Capsal, Appl. Therm. Eng. 2013, 57, 33.
- [40] Z. Xie, G. Sebald, D. Guyomar, Appl. Phys. Lett. 2015, 107, 081905.

- [41] Z. Xie, G. Sebald, D. Guyomar, Phys. Lett. A 2017, 381, 2112.
- [42] D. Črešnar, N. Derets, M. Trček, G. Skačej, A. Rešetič, M. Lavrič, V. Domenici, B. Zalar, S. Kralj, Z. Kutnjak, B. Rožič, J. Phys. Energy 2023, 5, 045004.
- [43] G. Skačej, Lig. Cryst. 2018, 45, 1964.
- [44] B. R. Donovan, H. E. Fowler, V. M. Matavulj, T. J. White, Angew. Chemie - Int. Ed. 2019, 58, 13744.
- [45] J. A. Herman, J. D. Hoang, J. M. McCracken, T. J. White, Macromolecules 2024, 52, 664.
- [46] A. F. Senyurt, H. Wei, C. E. Hoyle, S. G. Piland, T. E. Gould, Macromolecules 2007, 40, 4901.
- [47] M. Sahin, S. Ayalur-Karunakaran, J. Manhart, M. Wolfahrt, W. Kern, S. Schlögl, Adv. Eng. Mater. 2017, 19, 1600620.
- [48] C. E. Hoyle, A. B. Lowe, C. N. Bowman, Chem. Soc. Rev. 2010, 39, 1355
- [49] M. O. Saed, E. M. Terentjev, Sci. Rep. 2020, 10, 6609.